Production of medical radioisotopes ^{51}Cr, ^{62,64}Cu, and ^{99m}Tc by laser-induced photonuclear reactions*

Xuan Pang (庞萱)[1] Di Wu (吴笛)[2,3†] Bao-Hua Sun (孙保华)[1‡]
Mei-Zhi Wang (王美植)[2,3] Hao-Yang Lan (蓝浩洋)[2,3] Yu-Hui Xia (夏宇辉)[2,3]
Zhe-Nan Wang (王哲男)[2,3] Xin-Lu Xu (徐新路)[2,3] Xue-Qing Yan (颜学庆)[2,3]

[1]School of Physics, Beihang University, Beijing 100191, China
[2]State Key Laboratory of Nuclear Physics and Technology, School of Physics, CAPT, Peking University, Beijing 100871, China
[3]Beijing Laser Acceleration Innovation Center, Beijing 101407, China

Abstract: Laser-driven bremsstrahlung photon sources offer a promising approach to producing medical radioisotopes by photonuclear reactions. In this work, we report new activation measurements of ^{nat}Cr, ^{nat}Cu, and ^{nat}Ru using laser-driven bremsstrahlung at Peking University's Compact Laser Plasma Accelerator laboratory. The 200 TW laser was utilized with a 0.2 Hz repetition frequency. Activities of 2.27 Bq for ^{51}Cr, 5110 Bq for ^{62}Cu, 53.9 Bq for ^{64}Cu, and 16.4 Bq for ^{99m}Tc are achieved after irradiation for 20−30 min, using targets with a thickness of 2 mm. These crucial data, together with dedicated Monte Carlo simulations, enable a realistic evaluation to address the increasing demand in nuclear medicine. It is found that utilizing a repetition frequency of 100 Hz for the 200 TW laser and 10-cm-thick targets can satisfy the clinical diagnostic requirements of a typical activity of MBq for the isotopes of interest.

Keywords: medical radioisotope, photonuclear reaction, laser-driven bremsstrahlung, Monte-Carlo simulation

DOI: 10.1088/1674-1137/ae32fa **CSTR:** 32044.14.ChinesePhysicsC.50044003

I. INTRODUCTION

Diagnostic and therapeutic procedures using radioisotopes are now routine in the field of medicine. The relevant radioisotopes are typically produced in nuclear reactors or cyclotrons. In comparison, photonuclear reactions produce less heat owing to lower gamma-induced energy deposition, allowing the use of thicker targets with reduced cooling requirements [1]. Furthermore, they allow simultaneous multi-target irradiation [2], maximizing γ-beam utilization for the efficient production of various radioisotopes, including novel isomers [3, 4] that traditional methods cannot produce.

Over recent decades, with the rapid development of high-intensity and high-repetition-frequency laser systems, photonuclear reactions using these systems have been considered to be promising methods for producing radioisotopes [5]. In laser-driven bremsstrahlung photon sources, electrons are accelerated by ultrafast laser pulses. The accelerated electrons bombard a bremsstrahlung converter, leading to photon emission and subsequent photonuclear reactions with the target material. The efficient production of radioisotopes relies on the enhancement of photonuclear cross sections in the vicinity of the giant dipole resonance (GDR), which reaches a maximum at several MeV to a few tens of MeV. The safety and miniaturization of laser systems enable the production of radioisotopes closer to hospitals, thereby reducing their loss during transportation. Moreover, the narrow focal spot of the laser confines the reaction to a small area, significantly increasing the specific activity of the radioisotope. However, the method is still in an early stage of development.

In this work, we focus on the production of four medical radioisotopes: chromium-51 (^{51}Cr), copper-62 (^{62}Cu), copper-64 (^{64}Cu), and technetium-99m (^{99m}Tc). ^{51}Cr and ^{99m}Tc are typically produced in reactors, whereas ^{62}Cu and ^{64}Cu are generated by cyclotrons. ^{51}Cr is used to label red blood cells for monitoring and to quantify loss or bleeding of gastrointestinal proteins [6−8]. ^{62}Cu is a relatively short-lived β^+ emitter that is very suitable for positron emission tomography (PET) [9]. The radioiso-

Received 3 October 2025; Accepted 31 December 2025; Accepted manuscript online 1 January 2026
* Supported by the National Natural Science Foundation of China (12325506)
† E-mail: wdwd@pku.edu.cn
‡ E-mail: bhsun@buaa.edu.cn

tope ^{64}Cu, with an appropriate half-life of 12.7 h, has a low β^+ end-point energy of 0.65 MeV, which is comparable to that of ^{18}F ($T_{1/2}$ = 110 min), the most widely used positron emitter. It emits virtually no γ-ray. Additionally, its multiple decay modes make it suitable for combining PET and targeted therapy [10, 11]. Moreover, ^{64}Cu can form a "matched pair" with ^{62}Cu, enabling the measurement of uptake kinetics in an organ by PET imaging and allowing for precise dosimetric calculations [12, 13]. ^{99m}Tc is an ideal radioisotope for single-photon emission computed tomography (SPECT), making it the most common radioisotope used in diagnostic procedures [14, 15]. It accounts for approximately 80% of all nuclear medicine procedures and 85% of diagnostic scans worldwide [16]. However, a large majority of reactors producing ^{99m}Tc are expected to shut down by 2030 [17].

Currently, studies on laser-driven photonuclear reactions primarily focus on ^{62}Cu, ^{64}Cu, and ^{99m}Tc, which are generated by the reaction of ^{63}Cu$(\gamma, n)^{62}$Cu, ^{65}Cu$(\gamma, n)^{64}$Cu, and ^{100}Mo$(\gamma, n)^{99}$Mo/^{99m}Tc [18, 19]. In particular, relevant experiments have been performed at the XingGuangIII and CLAPA laser facilities [20, 21]. However, the achieved yields remain insufficient for clinical applications in humans, being adequate only for preclinical animal studies.

In this study, we aimed to evaluate the yield of ^{51}Cr, ^{62,64}Cu, and ^{99m}Tc radioisotopes via laser-induced photonuclear reactions, utilizing both experimental and simulation approaches. The experimental setup and data analysis are introduced in Section II. Subsequently, the yields of these medical radioisotopes are discussed and evaluated in Section III. Finally, a summary is given in Section IV.

II. EXPERIMENT AND DATA ANALYSIS

The experiments were performed at the 200 TW laser facility in the Compact Laser Plasma Accelerator (CLAPA) Laboratory at Peking University. The schematic layout of the experimental setup is shown in Fig. 1. Electrons are generated in the laser wake field acceleration (LWFA) by focusing the laser on a supersonic nozzle. Accelerated electrons collide with a converter, producing bremsstrahlung photons that subsequently undergo photonuclear reactions with the target nuclei. During the experiment, the laser system was operated at a relatively low energy, with a delivered energy of approximately 2.4 J to the target and a full-width at half-maximum (FWHM) duration of 30 fs. The laser beam was focused to 21 μm×23 μm (FWHM) at the nozzle. The gas jet is a 4 mm×1 mm rectangular supersonic nozzle, which can provide a flat density distribution for pure helium gas. The helium pressure is adjustable from 0 to 45 bar, and varying it can change the electron energy. A 40 μm Al foil and 60 μm Be window are used to block scattered light and seal the vacuum, respectively. A turbo integrating current transformer (Turbo-ICT) is used to measure the electron charge. The energy spectrum of electrons is measured by a 0.8 T magnetic spectrometer located 100 cm away from the gas jet. Fluorescent screens (Gd_2O_2S:Tb) at the entrance and exit of the magnet are used in conjunction with CCD cameras to record electron signals. No converter or experimental target is used for electron beam measurement. More details about the experiment setup and electron parameters are given in Refs. [22, 23].

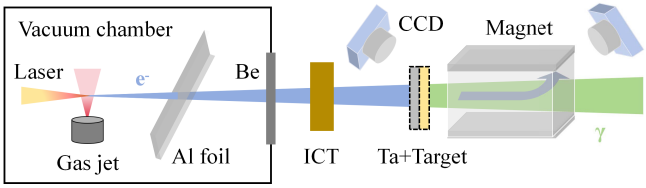

Fig. 1. (color online) Schematic layout of the experimental setup. Refer to the text for details.

In this experiment, the average electron charge per shot was 458 pC, with a peak energy of 200 MeV at gas pressures of 27 bar. The divergence angle was approximately 4.3 mrad. A Ta (99.9%) disk with a size of 2 cm×2 cm and thickness of 2 mm was employed as a bremsstrahlung converter. The monochromatic electron spectrum, as shown in Fig. 2, was determined using a magnetic spectrometer. It has limited acceptance, resulting in a truncated energy range up to 65 MeV. The bremsstrahlung γ-ray spectrum in Fig. 2 was obtained using the Geant4 toolkit [24−26] by taking the average electron spectrum of 100 continuous shots as input. The effect of the truncated low-energy electrons is considered to be negligible because of their low concentration.

The natural chromium (^{nat}Cr), copper (^{nat}Cu), and ruthenium (^{nat}Ru) targets had the same size as the Ta converter and were placed next to the converter. The relev-

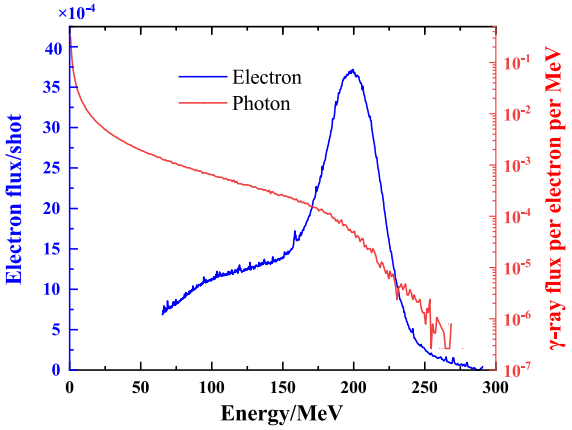

Fig. 2. (color online) Monochromatic electron spectrum measured by the magnetic spectrometer (blue line) and bremsstrahlung γ-ray spectrum per electron simulated using Geant4 toolkit [24−26] (red line).

ant data on the medical radioisotopes produced are shown in Table 1. The repetition frequency was set at 0.2 Hz to maintain the acceptable vacuum. ^{nat}Cu was irradiated for 20 min with approximately 241 laser shots. The irradiation time of ^{nat}Cr and ^{nat}Ru was 30 min, with about 361 laser shots per target. The transfer of the target to the offline measurement after irradiation took approximately 10 min.

The characteristic γ-ray spectra after irradiation were measured using two HPGe detectors with a relative efficiency of 40% (relative to the NaI(Tl) detector) and a 3×3 inch $LaBr_3$ detector. All detectors were placed in a low-background measurement system. The detector efficiencies were calibrated with standard ^{152}Eu and ^{60}Co sources. The summing coincidence correction was determined using Monte Carlo simulations [29] based on the actual geometry of the background detection system. The total offline measurement time was approximately 28 h for ^{nat}Cu and 24 h for ^{nat}Ru. For the ^{nat}Cr target, offline measurements were performed a total of 7 times within 60 days after irradiation, each with a duration of 16–40 h. As shown in Fig. 3, three characteristic peaks at energies of 320.1, 511, and 140.5 keV from the decay of ^{51}Cr, ^{62,64}Cu, and ^{99m}Tc were easily distinguished. The peaks of the background spectrum in Fig. 3(a) and Fig. 3(c) are rooted in the decays of actinides in the environment. The broad-energy continuum of bremsstrahlung enables the simultaneous activation of multiple photonuclear reaction channels. In addition to the contribution of ^{62,64}Cu, ^{60,61}Cu can induce β^+ decay and then emit 511 keV γ-rays. The cross sections of photoneutron reactions that generate these Cu isotopes are shown in Fig. 4. The ^{63}Cu$(\gamma,2n)$ reaction is the dominant source of ^{61}Cu, whereas the cross sections for other reaction channels producing ^{60,61}Cu are both significantly smaller (< 0.5 mb). Compared with the half-life of ^{64}Cu ($T_{1/2}$ = 12.70 h), the shorter half-lives of ^{61}Cu (3.34 h) and ^{60}Cu (23.74 min) ensure their complete decay within approximately 15 h after irradiation. Therefore, they do not interfere with the subsequent decay measurement of ^{64}Cu. For ^{62}Cu ($T_{1/2}$ = 9.67 min), within five half-lives of its decay, the contribution of 511 keV γ-rays originating from ^{60,61}Cu accounts for only about 1%, which is negligible within statistical uncertainties.

Based on the energy spectra measured at different time periods, the activity at time t can be calculated as follows:

$$A(t) = \frac{\lambda \Delta N \mathrm{e}^{-\lambda t}}{\mathrm{e}^{-\lambda t} - \mathrm{e}^{-\lambda(t+\Delta T)}}, \tag{1}$$

where ΔN is the characteristic peak count after background subtractions within the measurement time ΔT. The initial activity A_0 of the radioisotope can be deduced using an exponential fit to the $A(t)$. As shown in Fig. 3(b), both the decays of ^{62}Cu and ^{64}Cu contribute to the 511 keV peak. The initial activities can be determined using double-exponential fitting, given their very different half-lives. The corresponding compounds are displayed in Fig. 3(d). The steep beginning of the curve is primarily due to the rapid decay of ^{62}Cu, whereas the flat part is primarily attributed to the slow decay of ^{64}Cu. The activity at the initial time $t = 0$ in Fig. 3(d) corresponds to the activity at the end of irradiation.

For laser-driven γ-rays with low repetition frequencies, the total yield N of the product at the end of irradiation can be derived using the following equation:

$$N = \sum_{i=1}^{n} Y_i \exp(-\lambda(n-i)/f), \tag{2}$$

where n is the total number of shots, λ is the decay constant of the reaction product, f is the repetition frequency, and Y_i is the yield of the i-th shot. The experimental results are summarized in Table 2. The experimental single-shot yield was calculated as the total yield divided by the number of shots. The total uncertainty included uncertainties in statistical fluctuations, calibration of the detection efficiency, the half-life and decay branching ratio, and γ-ray absorption in the target. The γ-ray absorption in

Table 1. Decay properties of medical radioisotope ^{51}Cr, ^{62,64}Cu, and ^{99m}Tc and information of the corresponding photonuclear reaction. The first column represents the target in the photonuclear reaction. The natural abundance of the target is denoted as *Abu.*. The third column indicates the type of photonuclear reactions. The produced medical radioisotopes are characterized by the half-lives $T_{1/2}$ and decay modes. Here, $\%\varepsilon$ represents the probabilities of nuclear decay via electron capture or β^+ decay. $\%IT$ represents the probabilities of nuclear decay via isomeric transitions. The characteristic γ-ray energy in the decay, as well as the branching ratio intensity, are also provided. The last column indicates whether experimental data for the photonuclear reaction cross section are available in the EXFOR database [27]. The data were obtained from Ref. [28].

Target isotope	*Abu.* (%)	Reaction	Product	$T_{1/2}$	Decay mode	γ-ray energy/keV	Intensity (%)	EXFOR data
^{52}Cr	83.79	(γ, n)	^{51}Cr	27.70 d	$\%\varepsilon = 100$	320.1	10	Yes
^{63}Cu	69.15	(γ, n)	^{62}Cu	9.67 min	$\%\varepsilon = 100$	511	196	Yes
^{65}Cu	30.85	(γ, n)	^{64}Cu	12.70 h	$\%\varepsilon = 61.5$	511	35	Yes
^{100}Ru	12.60	(γ, p)	^{99m}Tc	6.01 h	$\%IT = 99.99$	140.5	89	No

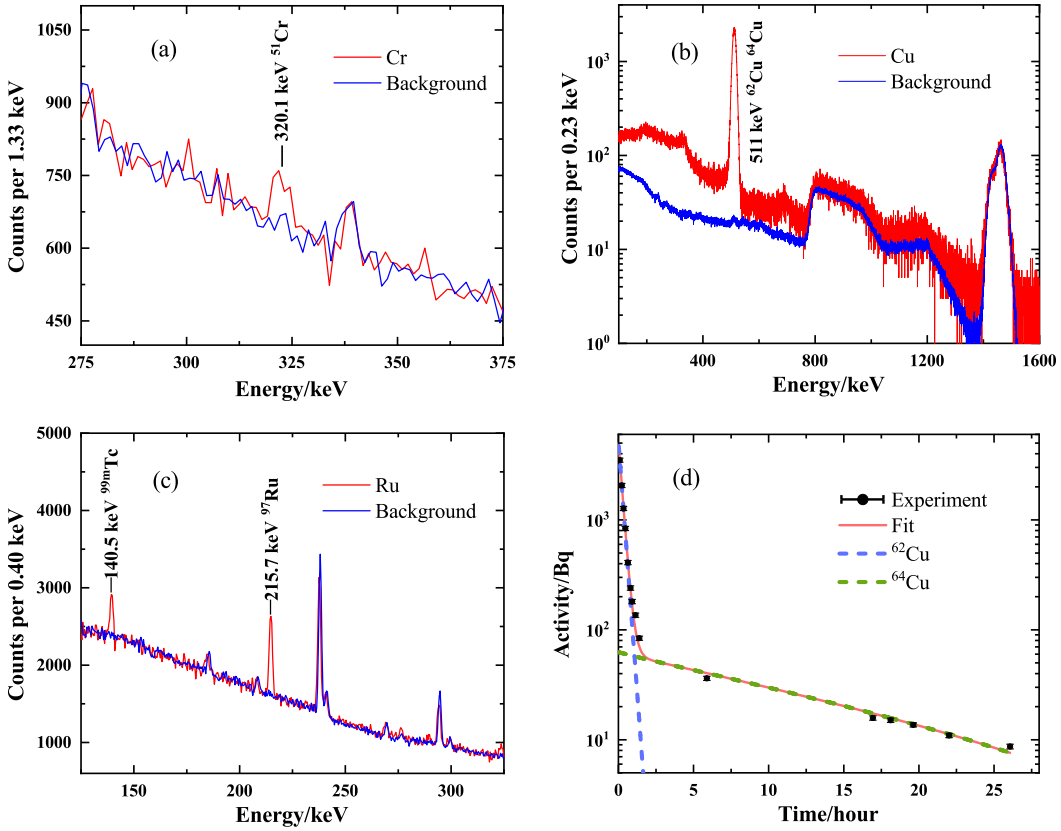

Fig. 3. (color online) Energy spectra of the irradiated ^{nat}Cr target (a), ^{nat}Cu target (b), and ^{nat}Ru target (c). The measurement times for spectra (a), (b), and (c) were 16.16 h, 287.26 s, and 12.24 h, respectively. The activity curve of ^{nat}Cu (d) was contributed by ^{62}Cu and ^{64}Cu. The energy spectra for ^{nat}Cr and ^{nat}Ru were measured using a HPGe detector, whereas the energy spectrum for ^{nat}Cu was obtained with a $LaBr_3$ detector. The background spectra were normalized by the measurement time and are shown in panels (a)–(c).

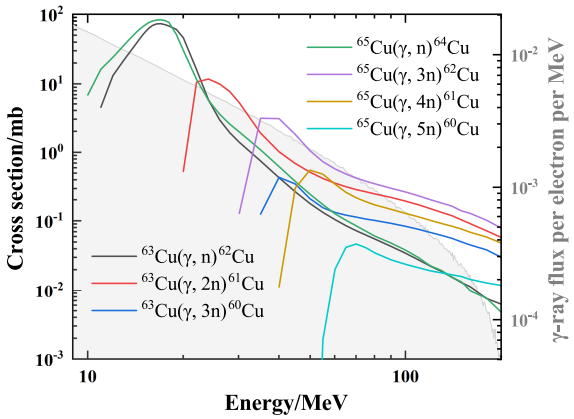

Fig. 4. (color online) Cross sections of photoneutron reactions for ^{63,65}Cu. The data were derived from the TENDL-2023 library [30, 31]. The gray area represents the bremsstrahlung spectrum as indicated by the red line in Fig. 2.

targets was also corrected. With a repetition frequency of 0.2 Hz, irradiation of 2-mm-thick natural targets for 20 min yielded activities of 5110 Bq for ^{62}Cu and 53.9 Bq for ^{64}Cu, whereas for 30 min, activities of 2.27 Bq for ^{51}Cr and 16.4 Bq for ^{99m}Tc were yielded. Although the experimental results demonstrate the viability of producing medical radioisotopes via laser-driven bremsstrahlung sources, the achieved activity is much lower than that required for clinical applications (MBq~GBq).

III. SIMULATION AND EVALUATION

Various parameters, such as electron current, number of shots, converter, and target size, limit the yield of medical radioisotopes via laser-induced photonuclear reactions. To optimize the production system, we performed Monte Carlo simulations using the Geant4 toolkit (version 11.0.3) [24–26]. The precision of the simulation was constrained by the available nuclear data, with the photonuclear reaction cross section being the key factor. Cross-section data are essential for determining the optimal energy range, predicting radioisotope yields, and estimating impurity levels. In Geant4, the cross sections for photonuclear reactions can be provided by the G4GammaNuclearXS (G4GNXS), G4PhotoNuclearCrossSection (G4PNCS), or LEND model. However, the photonuclear reaction cross sections obtained by the G4GNXS and G4PNCS classes are notably inconsistent with existing experimental data [32]. Although the LEND model

Table 2. Experimental and simulated results of the irradiated 2-mm-thick Cr, Cu, and Tc natural targets. The third and fourth columns show the experimentally measured activity and resulting single-shot yield for a target thickness of 2 mm, respectively. The fourth and fifth columns represent the experimental single-shot yield calculated by dividing the total yield by the number of shots and the simulated single-shot yield from the Monte Carlo with the same irradiated conditions, respectively. The last column indicates the evaluated single-shot results in the simulation with a target thickness of 10 cm. In the simulations, the photonuclear reaction cross sections were taken from the TENDL-2023 library [30].

Irradiated target	Product	Exp. activity/Bq	Single-shot yield	Sim. single-shot yield	Eval. single-shot yield
^{nat}Cr	^{51}Cr	2.27±0.16	(2.49±0.18)×10^4	2.78×10^4	8.47×10^5
^{nat}Cu	^{62}Cu	(5.11±0.21)×10^3	(2.95±0.12)×10^4	4.18×10^4	9.44×10^5
	^{64}Cu	53.9±4.8	(1.07±0.09)×10^4	1.28×10^4	2.89×10^5
^{nat}Ru	^{99m}Tc	16.4±1.4	(1.71±0.14)×10^3	2.15×10^3	6.50×10^4

agrees well with experimental data, it can only provide data with energies below 20 MeV. Currently, significant challenges remain in data scarcity and quality on photonuclear reactions, particularly for the (γ, p) reaction channel.

The TENDL-2023 library [30, 31] is one of the established references in nuclear data libraries. It is based on both default and adjusted TALYS calculations [33] and is used worldwide for analyzing and predicting nuclear reactions. In this work, we adapted the TENDL-2023 library into Geant4 using the Geant4-GENBOD toolkit [32]. The simulation algorithm is detailed in Ref. [34].

Table 2 presents the simulated and evaluated results of the single-shot yield. Under the same experimental conditions, the simulated single-shot yield agreed with experimental data within a factor of 1.5. The observed discrepancies may result from shot-to-shot instabilities in laser acceleration and from differences between the cross sections in the TENDL-2023 library used in Geant4 and the actual photonuclear cross sections. In the evaluated case, a natural target thickness of 10 cm is used. Compared with thin targets, secondary reactions from Compton scattering and attenuation of gamma rays within the target must be considered. The wide spectrum of bremsstrahlung enables the simultaneous opening of multiple reaction channels. Table 3 summarizes the ratio of single-shot yield between the major byproduct isotopes and the desired medical radioisotope under the evaluated case, providing reference data for future applications. Although the yields of isotopes with different atomic numbers are relatively high, they can be readily separated via chemical methods [35−37]. For ^{nat}Ru, the yield of ^{99m}Tc is much lower than that of other byproducts. Therefore, using enriched ^{100}Ru targets could be considered to increase the yield in future production.

Figure 5 illustrates the relationship between product activity and repetition frequency. The irradiated time is three times the half-life of the products. After three half-lives of irradiation, the activity of the product reaches 88% of its saturation value. The gray area indicates the activity levels of ^{62}Cu and ^{64}Cu required for PET imaging [38, 39]. For the production of ^{62}Cu, a lower frequency (~600 Hz) is sufficient to satisfy the standards for PET imaging. With a half-life of 9.67 min for ^{62}Cu, its saturation activity is achieved within one hour, as shown in Fig. 6. ^{64}Cu is also a promising radionuclide for targeted radiotherapy, with a recommended therapeutic dose of 99 MBq/kg [40]. For a standard adult patient (60 kg), this corresponds to approximately 6 GBq of administered activity. However, as shown in Fig. 6, the saturated activity is not sufficient for the requirements of this clinical therapy.

Table 3. Ratio of single-shot yield between the major byproduct isotopes and the desired medical radioisotope (^{51}Cr for ^{nat}Cr, ^{62,64}Cu for ^{nat}Cu, and ^{99m}Tc for ^{nat}Ru) in the simulation with a natural target thickness of 10 cm. Specifically, the ratio is relative to ^{62}Cu in the case of ^{nat}Cu. The produced isotope is characterized by the half-life $T_{1/2}$.

Target	Isotope	$T_{1/2}$	Ratio (%)
^{nat}Cr	^{48}Cr	21.56 h	0.26
	^{49}Cr	42.3 min	5.26
	^{49}V	330 d	11.44
	^{50}V	stable	11.86
	^{51}V	stable	70.01
^{nat}Cu	^{61}Cu	3.34 h	7.77
	^{61}Ni	stable	13.86
	^{62}Ni	stable	51.38
	^{63}Ni	100.80 y	0.65
	^{64}Ni	stable	12.35
^{nat}Ru	^{93}Tc	2.78 h	3×10^2
	^{94}Tc	293 min	7×10^2
	^{95}Tc	19.26 h	4.6×10^3
	^{97}Tc	4.21×10^6 y	5.3×10^3
	^{95}Ru	1.61 h	7.2×10^3
	^{97}Ru	2.84 d	6.3×10^3
	^{103}Ru	39.25 d	1.34×10^4

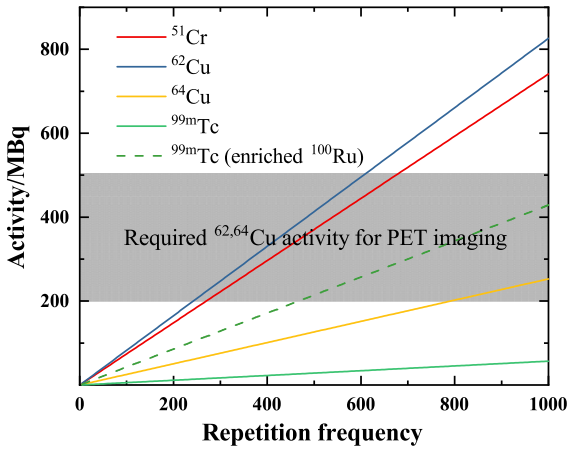

Fig. 5. (color online) Activity (in the unit of MBq) of ^{51}Cr, ^{62,64}Cu, and ^{99m}Tc versus repetition frequency (in the unit of Hz). The irradiated time is three times the half-life of radioisotopes. The gray area shows the required activities for PET. All the solid lines represent the expected activities from the relevant targets. The dotted line represents the available activity of ^{99m}Tc when using a 95% enriched ^{100}Ru target.

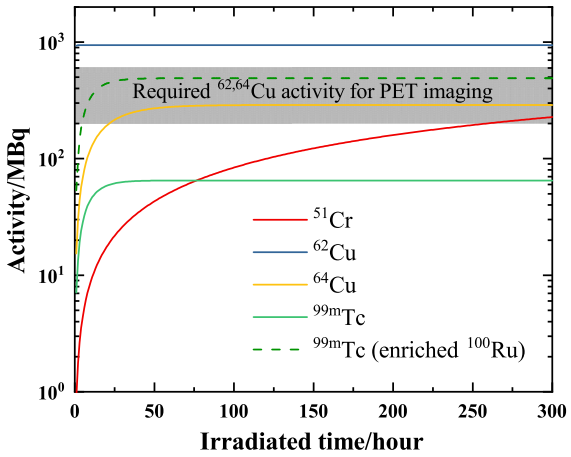

Fig. 6. (color online) Same as Fig. 5 but as a function of irradiation time (in hours). The repetition frequency is set to 1 kHz.

Red blood cells radiolabeled with ^{51}Cr are used to identify hemolytic anemia. In a clinical case, 4.07 MBq of ^{51}Cr-sodium chromic was used [8]. As shown in Fig. 6, only 20 h of irradiation is sufficient to reach the required level for a clinical trial.

^{99m}Tc is a commonly used imaging agent for SPECT imaging. The required activity varies depending on the purpose of clinical treatment. Brain perfusion imaging typically employs activities of 555–1110 MBq, with 740 MBq serving as the standard [41]. For bone scintigraphy in adults, the average activity administered by a single intravenous injection should be 500 MBq (300–740 MBq) [42]. Myocardial perfusion imaging uses an administered activity of 500 MBq for a standard examination [43]. In contrast, pulmonary perfusion scintigraphy employs a reduced activity of 200 MBq [44]. Currently, its saturation activity is approximately 65 MBq. When a 95% enriched ^{100}Ru target is employed, the achievable activity of ^{99m}Tc can reach 500 MBq. Furthermore, the required activity level for SPECT can be attained either by utilizing multiple synchronized lasers or by increasing the repetition frequency.

IV. SUMMARY

In this study, we performed activation measurements using the 200 TW laser facility at the CLAPA laboratory. Natural Cr, Cu, and Ru targets were irradiated for 20–30 min at a repetition frequency of 0.2 Hz. We obtained an activity of 2.27 Bq for ^{51}Cr, 5110 Bq for ^{62}Cu, 53.9 Bq for ^{64}Cu, and 16.4 Bq for ^{99m}Tc. However, the achieved activity is far from being suitable for clinical usage. To bridge this gap, we evaluated potential production using simulations employing cross sections from the TENDL-2023 library. With a natural target thickness of 10 cm and frequency of several hundred Hz, the simulated results could reach several 100 MBq for ^{51}Cr and ^{62,64}Cu, meeting clinical application requirements. For ^{99m}Tc, if a 95% enriched ^{100}Ru target is employed, the activity can reach 500 MBq, which is sufficient for clinical SPECT imaging.

Currently, the stable and continuous operation of a kilohertz laser-plasma accelerator has been reported [45]. However, the peak energy of the electron bunches is only 2.5 MeV, which results in a bremsstrahlung source with photon energies significantly below the (γ,n) and (γ,p) reaction thresholds for most nuclei. At high peak power levels, such as 200 TW in the CLAPA laboratory, increasing the repetition frequency poses significant challenges to the thermal resistance and damage of laser gain medium and mirror materials. Additionally, maintaining electron beam stability remains a critical problem. Another type of laser-driven gamma source, which employs laser Compton scattering (LCS) technology, may have the potential to produce medical radioisotopes at a clinical scale [46, 47], for example, at the newly built Shanghai Laser Electronic Gamma Source (SLEGS) [48, 49] and the upcoming Extreme Light Infrastructure – Nuclear Physics facility (ELI-NP) [50].

References

[1] D. Habs and U. Köster, Appl. Phys. B **103**, 501 (2011)
[2] Y. X. Yang, W. J. Zhao, X. G. Cao *et al.*, Radiat. Phys. Chem. **218**, 111599 (2024)
[3] H. Y. Lan, D. Wu, J. X. Liu *et al.*, Nucl. Sci. Tech. **34**, 74

(2023)
[4] W. T. Pan, T. Song, H. Y. Lan *et al*., Appl. Radiat. Isot. **168**, 109534 (2021)
[5] Z. L. Sun, AIP Advances **11**, 040701 (2021)
[6] A. Freud, A. Canfi, and E. Ben-Hur, Int. J. Radiat. Biol. **63**, 651 (1993)
[7] D. M. Mock, G. L. Lankford, J. A. Widness *et al*., Transfusion **39**, 156 (1999)
[8] B. W. Audrey and V. G. Vesper, J. Nucl. Med. Technol. **36**, 95 (2008)
[9] P. J. Blower, J. S. Lewis, and J. Zweit, Nucl. Med. Biol. **23**, 957 (1996)
[10] X. K. Sun and C. J. Anderson, Method Enzymol. **386**, 237 (2004)
[11] C. J. Anderson and R. Ferdani, Cancer Biother. Radiopharm. **24**, 379 (2009)
[12] A. Bockisch, J. Nucl. Med. Mol. Imaging **38**, 1 (2011)
[13] S. M. Qaim, B. Scholten, and B. Neumaier, J. Radioanal. Nucl. Chem. **318**, 1493 (2018)
[14] S. Banerjee, M. R. Ambikalmajan Pillai, and N. Ramamoorthy, Semin. Nucl. Med. **31**, 260 (2001)
[15] A. Duatti, Nucl. Med. Biol. **92**, 202 (2021)
[16] World Nuclear Association, Radioisotopes in Medicine, https://world-nuclear.org/information-library/non-power-nuclear-applications/radioisotopes-research/radioisotopes-in-medicine, retrieved 10th September 2024, .
[17] *IAEA Annual Report for 2021*, Tech. Rep. (Vienna: IAEA, 2022).
[18] A. D. Roberts, C. G. R. Geddes, N. Matlis *et al*., Appl. Radiat. Isot. **96**, 122 (2015)
[19] Z. G. Ma, H. Y. Lan, W. Y. Liu *et al*., Matter Radiat. Extremes **4**, 064401 (2019)
[20] Z. W. Cao, W. Qi, H. Y. Lan *et al*., Plasma Phys. Control. Fusion **65**, 055007 (2023)
[21] J. Y. Zhang, D. Wu, H. Y. Lan *et al*., Nucl. Sci. Tech. **35**, (2024)
[22] D. Wu, H. Y. Lan, J. Y. Zhang *et al*, arXiv: 2209.13947
[23] M. Z. Wang, D. Wu, H. Y. Lan *et al*., Nucl. Phys. A **1043**, 122834 (2024)
[24] S. Agostinelli, J. Allison, K. Amako *et al*., Nucl. Instrum. Methods A **506**, 250 (2003)
[25] J. Allison, K. Amako, J. Apostolakis *et al*., IEEE Tran. Nucl. Sci. **53**, 270 (2006)
[26] J. Allison, K. Amako, J. Apostolakis *et al*., Nucl. Instrum. Methods A **835**, 186 (2016)
[27] Experimental Nuclear Reaction Data (EXFOR), https://www-nds.iaea.org/exfor/, retrieved 23th September 2024.
[28] NuDat 3 database, https://www.nndc.bnl.gov/nudat3/, retrieved 23th September 2024.
[29] L. C. He, L. J. Diao, B. H. Sun *et al*., Nucl. Instrum. Methods A **880**, 22 (2018)
[30] A. J. Koning and D. Rochman, Nucl. Data Sheets **113**, 2841 (2012)
[31] A. J. Koning, D. Rochman, J. Sublet *et al*., Nucl. Data Sheets **155**, 1 (2019)
[32] W. Luo, H. Y. Lan, Y. Xu *et al*., Nucl. Instrum. Methods Phys. Res. A **849**, 49 (2017)
[33] A. J. Koning, S. Hilaire, and S. Goriely, Eur. Phys. J. A **59**, 131 (2023)
[34] W. Luo, M. Bobeica, I. Gheorghe *et al*., Appl. Phys. B **122**, 8 (2016)
[35] B. Y. Wu, C. P. Liu, C. Y. Fu *et al*., Chem. Eng. J. **373**, 1030 (2019)
[36] Y. Xue, Y. X. Hua, J. J. Ru *et al*., Adv. Powder Technol. **32**, 2791 (2021)
[37] S. Uchida and K. Tagami, Anal. Chim. Acta **357**, 1 (1997)
[38] T. Z. Wong, J. L. Lacy, N. A. Petry *et al*., Am. J. Roentgenol. **190**, 427 (2008)
[39] T. Zhang, S. K. Das, D. R. Fels *et al*., Am. J. Roentgenol. **201**, W698 (2013)
[40] K. Ito, Y. Narita, M. Hiroki *et al*., J. Nucl. Med. **66**, 2510946 (2025)
[41] Ö. L. Kapucu, F. Nobili, A. Varrone *et al*., Eur. J. Nucl. Med. Mol. Imaging **36**, 2093 (2009)
[42] T. Van den Wyngaert, K. Strobel, W. U. Kampen *et al*., Eur. J. Nucl. Med. Mol. Imaging **43**, 1723 (2016)
[43] H. J. Verberne, W. Acampa, C. Anagnostopoulos *et al*., Eur. J. Nucl. Med. Mol. Imaging **42**, 1929 (2015)
[44] Committee for Medicinal Products for Human Use (CHMP), *Guideline on core SmPC and package leaflet for technetium* (^{99m}Tc) *macrosalb*, Tech. Rep. (London: European Medicines Agency, 2016)
[45] L. Rovige, J. Huijts, I. Andriyash *et al*., Phys. Rev. Accel. Beams **23**, 093401 (2020)
[46] Y. N. Gu, W. J. Zhao, X. G. Cao *et al*., Nucl. Sci. Tech. **35**, 155 (2024)
[47] X. Pang, B. H. Sun, L. H. Zhu *et al*., Nucl. Sci. Tech. **34**, 187 (2023)
[48] H. W. Wang, G. T. Fan, W. Q. Shen *et al*., Nucl. Phys. News **33**, 17 (2023)
[49] H. W. Wang, G. T. Fan, L. X. Liu *et al*., Nucl. Sci. Tech. **33**, 87 (2022)
[50] D. Filipescu, A. Anzalone, D. L. Balabanski *et al*., Eur. Phys. J. A **51**, 185 (2015)